The proton motive force determines *Escherichia coli*'s robustness to extracellular pH

Guillaume Terradot [1], **Ekaterina Krasnopeeva** [1,2], **Peter S. Swain** [1*], **Teuta Pilizota** [1*]

[1] Centre for Synthetic and Systems Biology, King's Buildings, EH9 3FF, University of Edinburgh, Edinburgh, UK

[2] Current address: Institute of Science and Technology Austria, Am Campus 1, 3400 Klosterneuburg, Austria

Maintaining intracellular homeostases is a hallmark of life, and key physiological variables, such as cytoplasmic pH, osmotic pressure, and proton motive force (PMF), are typically interdependent. Developing a mathematical model focused on these links, we predict that *Escherichia coli* uses proton-ion antiporters to generate an out-of-equilibrium plasma membrane potential and so maintain the PMF at the constant levels observed. The strength of the PMF consequently determines the range of extracellular pH over which the cell is able to preserve its near neutral cytoplasmic pH. In support, we concurrently measure the PMF and cytoplasmic pH in single cells and demonstrate both that decreasing the PMF's strength impairs *E. coli*'s ability to maintain its pH and that artificially collapsing the PMF destroys the out-of-equilibrium plasma membrane potential. We further predict the observed ranges of extracellular pH for which three of *E. coli*'s antiporters are expressed, through defining their cost by the rate at which they divert imported protons from generating ATP. Taken together, our results suggest a new perspective on bacterial electrophysiology, where cells regulate the plasma membrane potential by changing the activities of antiporters to maintain both the PMF and cytoplasmic pH.

bacteria | pH | homeostasis | electrophysiology | mathematical modeling | membrane potential | antiporters

Correspondence: ***teuta.pilizota@ed.ac.uk and peter.swain@ed.ac.uk***

Internally, living cells differ from their environment and often maintain their intracellular properties within a restricted range – the phenomenon of homeostasis. For example, cytoplasmic pH (pH_i) is kept closed to neutral in organisms across all kingdoms of life, from archaea and eubacteria [1] to mammalian cells [2], likely because of the effect of pH on the stability and function of proteins [3].

Neutralophilic bacteria, such as *Escherichia coli*, maintain intracellular pH close to 7.5 in a range of values of extracellular pH (pH_e) [4]. Upon a sudden shift in pH_e from near neutral to acidic ($\sim$ 5.5), the pH of *E. coli's* cytoplasm has been shown initially to follow the change in pH_e, but then to quickly recover to $\sim$7.5 (Fig. 1A) [4, 5, 6]. This observation has been challenged, however, with reports of long-term changes to pH_i after a shift of extracellular pH (Fig. 1A) [7, 8, 9]. Explanations offered for this discrepancy include strain-to-strain differences and inaccuracies in calibrating and using pH sensors [7].

However, the homeostasis of pH is rarely studied in the context of the other physiological variables that pH influences. For example, the electrical potential across the membrane – the membrane voltage or membrane potential $\Delta\psi$ – is generated by the charge accumulated at the membrane, which includes protons. Further, the proton motive force (PMF), the electrochemical gradient of protons, is determined both by the $\Delta\psi$ and the difference between the intracellular and extracellular pH (ΔpH). More generally, the electrochemical gradients of all the other ions present in the cell – the ion motive forces (IMFs) – are influenced by the $\Delta\psi$ and so indirectly by protons. Protons can influence the osmotic pressure of the cell (Π) too, which depends on the difference between the extracellular and intracellular concentrations of all solutes [10]. The intertwined nature of these physiological variables suggests that we should study their maintenance together even if we wish to understand the homeostasis of only one.

To do so, we built a mathematical model of bacterial electrophysiology and found that the cell's ability to maintain pH_i as pH_e changes is determined by its PMF. This PMF depends on the extracellular environment, ion pumps, and charged intracellular molecules that cannot easily cross the plasma membrane. We measured *E. coli's* pH_i during shifts in extracellular pH at two different magnitudes of the PMF using previously developed single-cell assays [11]. Agreeing with the model, we find that pH_i is maintained at a given pH_e only if the absolute magnitude of the PMF is sufficiently high. Our results indicate a way to reconcile previous contradictory observations [4, 5, 6, 7, 8] – the measured cells may have had a different PMF. Finally, our model and experiments suggest that pH_i is not regulated directly, but is predominately controlled through the cell modulating its membrane potential upon changes in pH_e.

Results

A mathematical model provides a holistic view of intracellular homeostasis. To describe as simply as possible how pH_i is maintained, we developed a minimal mathematical model of cellular electrophysiology based on previous work [12] and comprising five species: protons (H^+), hydroxide ions (OH^-), a monovalent cation (C^+), a monovalent anion (A^-), and molecules that are captive and unable to cross the plasma membrane (Fig. 1B). All ions except captive ions leak across the plasma membrane [13], but H^+, C^+ and A^- may also be pumped.

We allow ions to be actively transported solely by proton antiporters – secondary pumps characterised by a specific stoichiometric ratio. For example, a cation antiporter with a sto-

ichiometric ratio of 2 moves two H^+ in and one C^+ out. We assume that the PMF, which powers the antiporters, is generated via two reactions, one typically occurring during cellular respiration and the other during fermentation. By including captive molecules, such as non-polymerised metabolites including glutamate – the most abundant [14], we partially account for some cellular processes not explicitly modelled. Finally, we assume that cells have been selected to maintain a constant PMF as reported across a range of growth rates [15, 16].

Mathematically, the electrochemical potential of an ion x, with an intracellular concentration of $[x_i]$ and an extracellular concentration of $[x_e]$, is defined as:

$$\Delta G_x = z_x \Delta\psi + \frac{RT}{F} \ln \frac{[x]_i}{[x]_e} \tag{1}$$

where z_x is the ion's valency, which we assume to be ± 1. Defining R as the gas constant, T as the temperature, F as Faraday's constant, and $\Delta\psi$ as the membrane potential, Eq. (1) is the free energy required to move an extracellular ion into the cell measured in volts. We will use ΔG_x interchangeably with the electrochemical potential of ions, or the ion motive force (IMF), and similarly use ΔG_{H^+} for the PMF:

$$\Delta G_{H^+} = \Delta\psi - \ln 10 \frac{RT}{F} \Delta\mathrm{pH} \tag{2}$$

where $\Delta\mathrm{pH} = \mathrm{pH}_i - \mathrm{pH}_e$.

A build-up of electrical potential across the membrane is enabled by its hydrophobicity, and, following others [17, 13], we assume that the charge accumulated in close proximity to the membrane is equivalent to the surface charge on a parallel-plate capacitor:

$$\Delta\psi = \frac{F}{SC_m} \underbrace{V \sum_x z_x [x]_i}_{Q_i} \tag{3}$$

where Q_i is the total intracellular charge. Q_i is only non-zero adjacent to the membrane and is equal and opposite in sign to the total extracellular charge Q_e, also only non-zero adjacent to the membrane. We denote the membrane capacitance as C_m and the cell's volume and surface area as V and S (*Supplementary Information*). For simplicity, and without any loss of generalisation – a rescaling is required otherwise, we assume that the cell's has no incompressible volume. In Eq. (3), we include captive molecules. Uncharged captive molecules ($z_x = 0$), although not contributing to $\Delta\psi$, do contribute to the cell's osmotic pressure.

Assuming all osmotic coefficients are equal to one, this osmotic pressure is given by the difference in total concentration across the membrane [13, 18]:

$$\Pi = RT \sum_x \Big([x]_i - [x]_e \Big). \tag{4}$$

Ionic concentrations change because ions move across the membrane

$$\frac{d[x]_i}{dt} = -\frac{d[x]_e}{dt} = j_x + \sum_n \sigma_{x,n} j_n \tag{5}$$

where j_x is the flux from leakage and j_n is the flux from pumping reaction n with a stoichiometric coefficient $\sigma_{x,n}$. We write the dependency of a reaction rate on the reaction's free energy ΔG as [19]:

$$j = j^+ \left(1 - e^{\frac{F}{RT}\Delta G_x} \right). \tag{6}$$

The rate j^+ is a function determined by the transport mechanism's kinetics, e.g. whether it is a two-step or four-step process [13]. For pumps, we assume that j^+ is a constant (for a given electrophysiological steady-state) [17]. For the leakage flux of ion x, we use

$$j_x^+ = \frac{S}{V} P_x x_e f_b(\Delta\psi) \tag{7}$$

where P_x the membrane's permeability to x, and the functional form of $f_b(\Delta\psi)$ changes with the choice of approximation [20] (*Supplementary Information*).

To allow the cell to generate energy, we first define the respirative regime by the coupling of the redox reaction $\mathrm{R}^\star \rightleftharpoons \mathrm{R}$, where $\mathrm{R}^\star$ is typically NADH, to the export of protons:

$$\mathrm{R}^\star + \sigma_{H^+,R} \mathrm{H}_i^+ \rightleftharpoons \mathrm{R} + \sigma_{H^+,R} \mathrm{H}_e. \tag{8}$$

Writing ΔG_{NADH} as the redox reaction's potential, then

$$\Delta G_R = \Delta G_{\mathrm{NADH}} - \sigma_{H^+,R} \Delta G_{H^+} < 0 \tag{9}$$

if protons are to be exported. These protons are used by the $\mathrm{F_1F}_o$ ATP synthase to generate ATP [21]:

$$\mathrm{ADP} + \sigma_{\mathrm{H},F_1F_o} \mathrm{H}_e \rightleftharpoons \mathrm{ATP} + \sigma_{\mathrm{H},F_1F_o} \mathrm{H}_i, \tag{10}$$

and for the flux of ATP to be positive, we require:

$$\Delta G_{F_1F_o} = \sigma_{H^+,F_1F_o} \Delta G_{H^+} - \Delta G_{\mathrm{ATP}} < 0. \tag{11}$$

Together Eq. (9) and Eq. (11) bound the magnitude of the PMF in the respirative regime:

$$\frac{\Delta G_{\mathrm{NADH}}}{\sigma_{H^+,R}} < \Delta G_{H^+} < \frac{\Delta G_{\mathrm{ATP}}}{\sigma_{H^+,F_1F_o}} \tag{12}$$

To estimate these limits, we use $\Delta G_{\mathrm{ATP}} \simeq$ -560 mV for exponentially growing cells respiring on glucose [14] and $\sigma_{H^+,F_1F_o} = 3.3$ [22] (*Supplementary Information*). For ΔG_R, we use -2290 mV from the Gibbs free energy of the half-reactions [23] and with 10 protons moved per NADH oxidised [24]. We thus find that

$$-229 \text{ mV} < \Delta G_{H^+} < -170 \text{ mV}. \tag{13}$$

The fermentative regime is simpler with $\mathrm{F_1F}_o$ hydrolysing ATP to export protons, which requires $\sigma_{H^+,F_1F_o} \Delta G_{H^+} > \Delta G_{\mathrm{ATP}}$ or

$$\Delta G_{H^+} > -170 \text{ mV}. \tag{14}$$

A caveat is that the free energy of ATP hydrolysis and the stoichiometric ratio σ_{H^+,F_1F_o} may change in different extracellular environments [25, 26], which would modify the value of the PMF that separates the respirative and fermentative regimes. We also note that apart from F_1F_o ATP-synthase operating in the fermentative regime, there are no known ATP-driven ion efflux pumps in *E. coli*, justifying our choice of active ion transport occurring solely through proton antiporters.

To change the extracellular environment, we start with water at pH 7 and add either an acid AH or a base COH to alter pH_e and salt CA to modify the ionic concentrations. We assume the environment equilibrates rapidly and is unchanged by the cell's activity so that the concentration of extracellular ions are both constant and fully determined (*Supplementary Information*).

Although we have considered only a single membrane and the envelope of *E. coli*, like other Gram-negative bacteria, has both an inner and an outer membrane [27], including such periplasmic effects does not qualitatively change our results. Any captive charged molecules in the periplasm create a periplasmic electrical potential, which augments the plasma membrane potential and generates a constant offset to the extracellular concentrations 'felt' at the inner membrane (*Supplementary Information* and Fig. S1).

Having developed the model, we now explore how changes in pH_e affect pH_i, $\Delta\psi$, and PMF.

The cell's PMF determines whether it maintains pH_i at different pH_e. We first note that for most microbes, including acidophiles and *E. coli*, the contribution from $[H^+]_i$ and $[OH^-]_i$ to $\Delta\psi$ is negligible – at most ± 3.5 mV compared to a $\Delta\psi \simeq -140$ mV [28] – because pH_i stays within the 6 to 8 range [1, 7].

Protons alone cannot therefore generate a substantial $\Delta\psi$, and although cells use energy to pump protons directly, it is the antiporters in our model that generate a physiological $\Delta\psi$ by moving ions in exchange for the protons pumped. We consider four types of antiporter (Fig. 1C), three of which have analogues in *E. coli*: ClcA [29], NhaB [30], and NhaA [31].

Our pumping reaction n in Eq. (5) is therefore the action of an antiporter a, which obeys

$$\sigma_{H^+,a}\,\mathrm{H}_e^+ + \sigma_{x,a}\,x_i \rightleftharpoons \sigma_{H^+,a}\,\mathrm{H}_i^+ + \sigma_{x,a}\,x_e. \qquad \textbf{(15)}$$

To export x, this reaction's ΔG should be negative:

$$\Delta G_{x,a} = \sigma_{H^+,a}\,\Delta G_{H^+} - \sigma_{x,a}\,\Delta G_x < 0. \qquad \textbf{(16)}$$

The export of x is balanced at steady state by its leakage across the membrane, implying that the leakage flux j_x must be positive and, from Eq. (6), $\Delta G_x < 0$. Combining this inequality with Eq. (16) implies

$$\frac{\sigma_{\mathrm{H}^+,a}}{\sigma_{x,a}}\Delta G_{\mathrm{H}^+} < \Delta G_x < 0 \qquad \textbf{(17)}$$

and the IMF, ΔG_x, is bounded.

By fixing the concentrations of extracellular ions, pH_e, and the charge and intracellular concentration of captive molecules, and by assuming that pH_i is neutral and that the PMF is kept constant, we are able to determine if these steady-state physiological conditions are compatible with the properties of a given antiporter. By compatible, we mean that Eq. (17) holds, and the antiporter is able to transport in a direction that maintains a steady state and balances leakage.

From the definition of the PMF, Eq. (2), specifying the pH_i and pH_e determines the membrane potential. Ignoring the negligible contributions of protons and hydroxide ions, Eq. (3) becomes

$$\Delta\psi \simeq \frac{FV}{SC_m}\Big(z_Y[Y]_i + [C^+]_i - [A^-]_i\Big) \qquad \textbf{(18)}$$

recalling that we consider only one type of cation and anion. Using Eq. (1), Eq. (18) can be written in terms of the extracellular concentrations

$$\begin{aligned}\Delta\psi \simeq \frac{FV}{SC_m}\Big(&z_Y[Y]_i + [C^+]_e\,\mathrm{e}^{\frac{F}{RT}(\Delta G_{\mathrm{C}^+} - \Delta\psi)} \\ &- [A^-]_e\,\mathrm{e}^{\frac{F}{RT}(\Delta G_{\mathrm{A}^-} + \Delta\psi)}\Big).\end{aligned} \qquad \textbf{(19)}$$

For a given antiporter, we find a range of values of the PMF and pH_e over which it is able to maintain a steady state with a neutral pH_i (Fig. 1D and S2). As an example of our methodology, consider an antiporter that exchanges cations for protons like NhaA. Anions are then only passively transported: $\Delta G_{A^-} = 0$ at steady state and in Eq. (19). For each set of physiological conditions, we test if the antiporter is compatible by determining if ΔG_{C^+}, found from Eq. (19), obeys Eq. (17). Alternatively, if our antiporter exchanges anions for protons like ClcA, then ΔG_{C^+} is zero at steady state, and we compare the ΔG_{A^-} with Eq. (17).

To understand why the range of PMF and pH_e is restricted, consider NhaA when $z_Y[Y]_i = 0$ in Eq. (19) and pH_e is 5.5 (Fig. 1D – black line). The corresponding ΔpH is fixed at 1.5 and contributes -90 mV to the PMF. NhaA exchanges cations and $\Delta G_{A^-} = 0$. Consequently, $[A_i]$ passively follows the membrane potential with $[A_i] = [A_e]\exp(\frac{F\Delta\psi}{RT})$, increasing if $\Delta\psi$ becomes more positive and vice versa.

With NhaA, steady states become impossible for sufficiently positive PMFs (Fig. 1D), which require a more positive $\Delta\psi$ for a fixed ΔpH from Eq. (2). A more positive $\Delta\psi$ increases $[A_i]$, which is passive for NhaA, and so, from Eq. (18), can only be generated if $[C_i]$ increases. This increase in $[C_i]$ and the more positive $\Delta\psi$ raises ΔG_{C^+} via Eq. (1) until the upper bound of Eq. (17) is reached, and cations begin to leak out of the cell. If $z_Y[Y]_i$ is negative rather than zero, then for a given (sufficiently positive) PMF and pH_e and neutral pH_i, which specify $\Delta\psi$, $[C_i]$ must be higher. These higher concentrations favour cations leaking from the cell and so lower

the $\Delta\psi$ and hence the PMF at which the upper bound of zero ΔG_{C+} is reached (Fig. 1D top and S3).

With NhaA, steady states also become impossible for sufficiently negative PMFs (Fig. 1D), which require a more negative $\Delta\psi$ for a fixed ΔpH. Such a $\Delta\psi$ decreases $[A_i]$ and so can only be generated if $[C_i]$ decreases. This decrease in $[C_i]$ and the more negative $\Delta\psi$ lowers ΔG_{C+}. Exporting cations becomes harder until the lower bound of Eq. (17) is reached. The export of cations then stops, preventing a steady state. Although a more negative PMF increases the free energy available to drive antiport, the corresponding decrease in $[C_i]$ dominates, and the overall free-energy change eventually becomes zero. If $z_Y[Y]_i$ is positive rather than zero, $[C_i]$ must be lower for a given PMF and pH$_e$. These lower concentrations make exporting cations harder, and so the point where the PMF is decreased sufficiently to stop export by the corresponding decrease in $[C_i]$ occurs at a higher PMF (Fig. 1D bottom and S3).

Importantly, the range of pH$_e$ over which the cell maintains a steady state increases if the PMF is more negative (Fig. 1D). The lower limit of pH$_e$ is determined by the upper bound of Eq. (17). When pH$_e$ decreases below pH$_i$ for a constant PMF, Eq. (2) implies that the cell generates a more positive membrane potential to maintain a steady state. For NhaA, $[C_i]$ increases, and the upper bound is passed when ΔG_{C+} becomes positive so that cations leak out of the cell. A more negative PMF for a given ΔpH decreases $\Delta\psi$ and so extends the lower limit of pH$_e$ by making it harder for cations to leak out. The upper limit of pH$_e$ is determined by the lower bound of Eq. (17). When pH$_e$ increases above pH$_i$ for a constant PMF, Eq. (2) implies that the cell generates a more negative membrane potential to maintain a steady state. For NhaA, $[C_i]$ decreases, and the lower bound is reached when ΔG_{C+} is so negative that the antiporter's export flux vanishes. A more negative PMF increases the free energy available to the protons driving export of cations and so extends the upper limit of pH$_e$.

We predict that pH$_i$ is maintained over the widest range of pH$_e$ in the respirative rather than the fermentative regime because the PMF is then more negative (Fig. 1D). This robustness to pH$_e$ comes at a cost. A more negative PMF will require the electron transport chain to export protons at a greater rate because the correspondingly more negative membrane potential will increase the import rate of protons by both the antiporters and leakage.

Finally, we note that without active pumping, ions will leak across the membrane and eventually $\Delta G_{A^-} = \Delta G_{C^+} = \Delta G_{H^+} = 0$, but $\Delta\psi$ will not vanish because of the captive charged molecules. These molecules, which have concentrations up to 300 mM [14], are able to generate a physiological $\Delta\psi$ if the extracellular environment has sufficiently low concentrations of extracellular cations and anions. If these concentrations are too high, however, a physiological $\Delta\psi$ would raise the cell's osmotic pressure above observed values – 0.3 to 3 atm [32, 33] (Fig. S4).

At pH$_e$ 5.5, *E. coli* maintains pH$_i$ if the PMF is sufficiently negative. To confirm the predicted role of PMF on the robustness of pH$_i$, we should measure PMF and pH$_i$ simultaneously in individual bacteria while controlling the magnitude of the PMF. We can do so by using the speed of the bacterial flagellar motor to indicate PMF and a ratiometric pH sensor (pHluorin [34]) to measure pH$_i$ [11, 12, 35].

The flagellar motor is a rotary nano-machine [36], and its speed is proportional to the PMF irrespective of its load [37, 38]. Measuring changes in the motor's speed is therefore equivalent to measuring the change in PMF. By attaching a cell to the surface of a cover slip [39] and a plastic bead to a genetically modified filament stub of the flagellum [40, 41, 42, 11, 35], we are able to measure the rotation of the motor labeled with the bead through placing the bead in a heavily attenuated optical trap and performing back-focal-plane interferometry (Fig. 2A) [43, 44]. The strains we use also express cytoplasmic pHluorin [11, 12, 35].

To change the PMF, we use a sealed tunnel-slide configuration [45, 42, 11], where cells eventually run out of oxygen and the magnitude of the PMF drops [46] (Fig. 2B). Although the timing of the drop varies between 20 and 30 min and depends on the concentration of cells on the tunnel-slide surface, as reported for a population of swimming cells [46], the characteristic step-like shape is conserved (Fig. S5).

We change pH$_e$ from 7.0 to 5.5 and observe pH$_i$, first at a higher absolute PMF that is maintained in the presence of oxygen and then at lower one when the oxygen in the tunnel-slide is depleted (arrows in Fig. 2B). The motor's speed, and hence the PMF, changes in these aerobic and anaerobic conditions (Fig. 2B & C).

As predicted (Fig. 1D), pH$_i$ is maintained over a wider range of pH$_e$ for the higher magnitude PMF in the aerobic environment compared to the lower magnitude PMF in the anaerobic environment (Fig. 2D).

Changing pH$_e$ to 5.5, the cytoplasm temporarily acidifies (Fig. 2F), but then recovers towards its initial value if the magnitude of the PMF is kept high by oxygen being present (Fig. 2E). As oxygen falls and the PMF's magnitude drops, pH$_i$ falls back to the value seen when pH$_e$ was first changed. If we alter pH$_e$ to below 5, we observe no dynamic recovery, and both the magnitude of the PMF and pH$_i$ drop permanently indicating that the gradient of protons across the membrane has collapsed (Fig. S6).

A ΔpH requires a PMF if antiporters regulate the membrane potential. If antiporters are the only pumps to export C^+ and A^-, our model's main prediction is that antiporters adjust $\Delta\psi$ to keep the PMF fixed and pH$_i$ near neutral. We emphasise that the antiporters do not act to maintain specific intracellular ionic concentrations, but only do so as a secondary effect while maintaining the PMF. In our model, antiporters will not export a proton to preserve pH$_i$ while keeping $\Delta\psi$ constant [47, 48, 1], but instead adjust $\Delta\psi$ to maintain the PMF.

A plausible alternative, however, is for cells to express an AT-

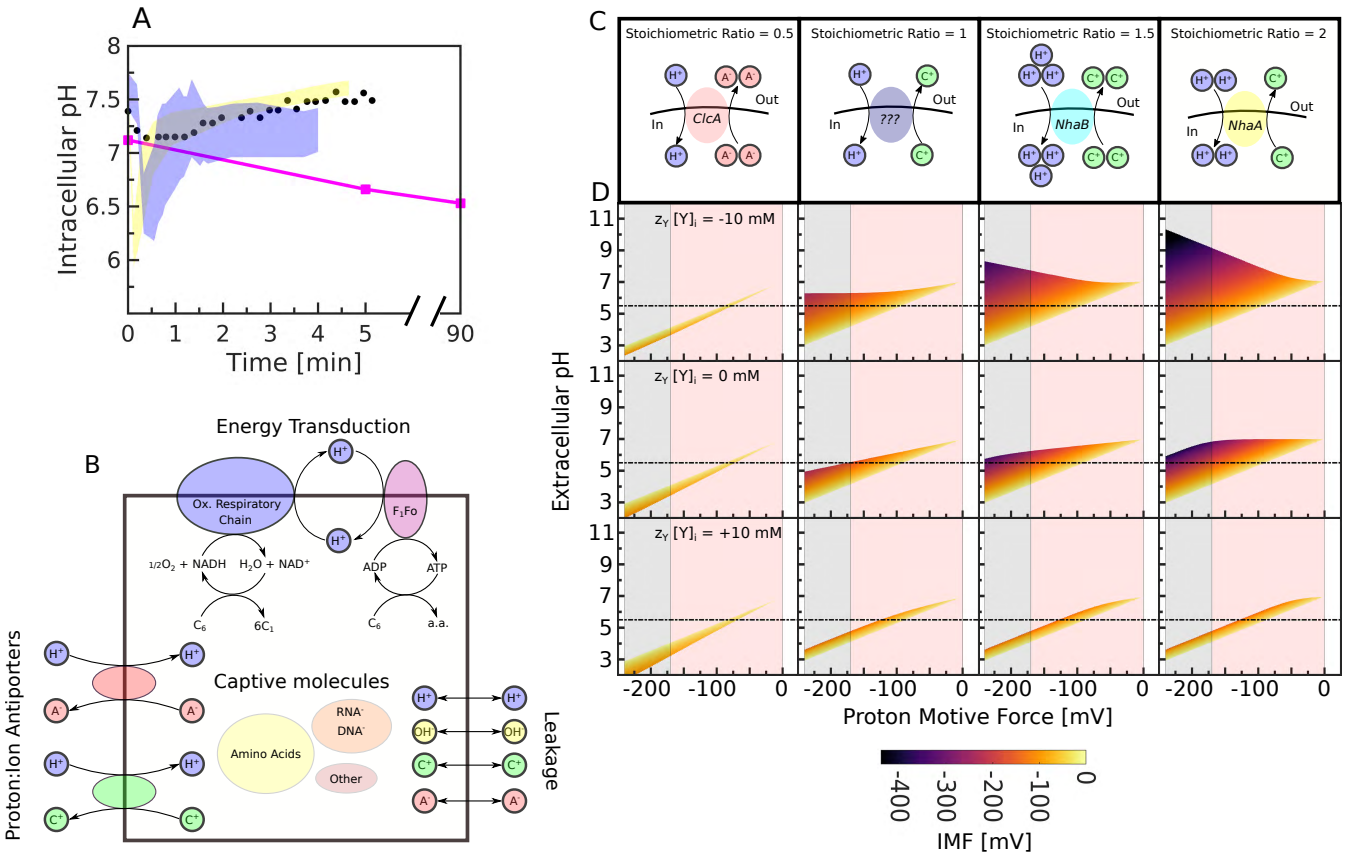

Fig. 1. A cell's ability to maintain pH_i over a range of pH_e is directly related to its PMF. (A) We reproduce experimental results on pH_i's homeostasis. Pink squares are for cells when pH_e is changed from 7.2 to 5.6 [7]. Black dots are population averages [4] for a pH_e shifted from 7.5 to 5.5, and the yellow [5] and blue [6] shaded areas show the range of pH_i measured in single cells for the same shift in pH_e. (B) A simplified model of *E. coli*'s electrophysiology. We distinguish two classes of chemical species contributing to the membrane potential – small ions, which both leak and are pumped across the membrane, and captive molecules, which cannot cross the membrane. Only two cations – protons and a representative cation C^+ – and two anions – hydroxide ions and an anion A^- – are included. The PMF is powered by either the electron transport chain or the F_1F_o ATPase. The concentrations of NADH, NAD^+, ATP, and ADP, and of extracellular ions are fixed. Proton-ion antiporters exchange protons for either C^+ or A^- and generate ionic motive forces. (C) We consider four antiporters. Their stoichiometric ratio is the ratio of the number of protons to the number of ions exchanged. (D) We plot the possible steady-state solutions for each antiporter for a given PMF between -240 mV and 0 mV, a pH_i of 7, and pH_e between 2 and 12. $[CA]_0 = 100$ mM, and we consider three values of the total captive charge, $z_Y Y_i$. The horizontal black line marks pH_e= 5.5. Grey shading shows values of the PMF expected for respiration and red shows the values expected for fermentation. The colour scale indicates the ionic motive force (IMF).

Pase that directly exports ions. Such pumps, although present in mammalian cells [49], are unreported for *E. coli* but they may exist, and so we sought an experiment to distinguish between pumping of ions by antiporters and by an ATPase. Selecting antiporters with stoichiometric ratios of 0.5, 1.5 and 2 and a hypothetical ATPase with a stoichiometric ratio of 0.5 (Fig. 3A), we determined how the steady-state ΔpH and $\Delta\psi$ change with the PMF in the model (Fig. 3B). Although fixing the PMF and $\Delta\psi$ determines ΔpH, it is only when Eq. (17) holds too that a steady state is possible.

The most notable difference between ion transport being powered by PMF or ATP is in the alkaline range at low magnitudes of the PMF. If $\Delta\psi$ is generated by proton-ion antiporters, then it is generated by the PMF powering these antiporters. When the PMF is zero, ΔpH is therefore proportional to the resulting equilibrated $\Delta\psi$, which is of small magnitude, and ΔpH is close to zero. In contrast, if $\Delta\psi$ is generated by an ATPase, then it is generated independently from the PMF and ΔpH need not be small when the PMF is zero.

To collapse the PMF experimentally, we treat cells in the alkaline regime with a protonophore (Fig. 3C), 100 μM carbonyl cyanide m-chlorophenylhydrazone (CCCP) [50, 51]. Changing pH_e to either 8.15 or 8.45, we see that the magnitude of the PMF drops and then collapses to zero when CCCP is added. Intracellular pH rises with the alkaline shift and then starts to recover, but ΔpH is close to zero with CCCP, as predicted by the antiporter model and assuming there is sufficient ATP available to power the ATPase. The recovery of pH_i upon the alkaline shift at the lower magnitude PMF (Figs. 3C) agrees with previous measurements [52]. If we use the known range of the PMF during respiration on glucose to estimate $\Delta\psi$ (Fig. S7), $\Delta\psi$ stays approximately constant during the alkaline shifts, supporting a previously reported small ~ 10 mV change [52].

If $\Delta\psi$ is generated by antiporters, we also do not expect a substantial $\Delta\psi$ in the absence of PMF, again consistent with our results (Fig. 3D). These findings contrast with those from mammalian cells, where $\Delta\psi$ is generated by a sodium-potassium ATPase [49] and can be determined by measuring ΔpH in the presence of CCCP [53, 54].

Interestingly, although we obtained data in the presence of

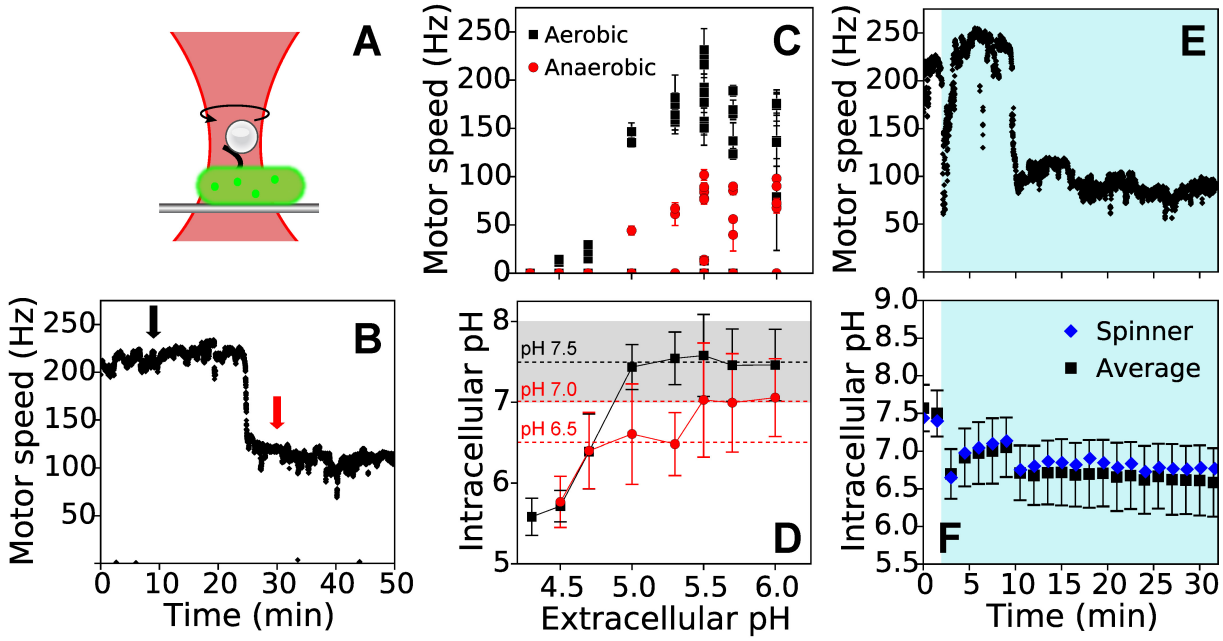

Fig. 2. At acidic pH_e, *E. coli* maintains neutral pH_i if the magnitude of the PMF is sufficiently high. (A) A schematic showing *E. coli* immobilised on a glass coverslip with a polystyrene bead attached to a 'sticky' stub of a bacterial flagellar filament. The bacterium is placed in the focus of a heavily attenuated laser to detect the position of the bead at high speeds. We use the flagellar motor's rotational speed as a proxy for PMF. The cell's cytoplasm is in green to illustrate that we concurrently monitor a fluorescent pH sensor. (B) An example of the motor speed from a single cell in a sealed tunnel-slide at pH_e=7.0 in 20 mM glucose. The sharp drop at $\sim$ 25 min occurs when oxygen is exhausted. The arrows show where we measure 'aerobic' (black) and 'anaerobic' (red) speeds. (C) The single-cell motor speed depends on pH_e. Speeds are calculated as the mean of a $\pm$ 45 s interval around the time points indicated in B. Error bars are standard deviations. (D) pH_i changes with pH_e and is calculated as the mean of 90 to 316 cells for the time points indicated in B. Error bars are standard deviations. Grey shading shows the region of pH_i homeostasis, between pH 7 and 8. (E) An example of single-cell motor speed upon shifting to pH_e=5.5. Initially cells are at pH_e=7, and then pH_e is changed to 5.5 at t= 2 min (blue shade) and the tunnel-slide is sealed. At the point where pH_e shifts, the bead rotated by the motor moves out of the laser's region of detection, due to flow, giving a loss of signal – the sharp drop in speed. (F) The dynamics of pH_i depends on the PMF. Blue diamonds show the cell from E; black squares show the mean and the standard deviation for all the cells in the field of view ($\sim$ 30). Blue shading indicates where pH_e is 5.5.

oxygen, the estimated PMF at which we observe pH_i recovering is in the fermentative regime (Fig. 3D)). As mentioned, we assume a fixed free energy and stoichiometric ratio of ATP hydrolysis, which could change at high pH_e. Alternatively, cells may switch to fermentation in alkaline stress.

The optimal choice of antiporter depends on extracellular pH. For a given PMF and pH_e, multiple different antiporters are able to maintain the same steady state (Fig. 1D), and we therefore wished to understand when a particular antiporter might be favoured.

Using one type of antiporter may be more or less costly than using another. We define this cost as the flux of protons that are neither directly involved in generating ATP during respiratory growth nor are actively pumped by F_1F_o during fermentative growth. These protons enter the cell via leakage and the antiporters. They are costly because they either could instead have been used to generate ATP during respiration or because they undermine F_1F_o's export of protons during fermentation. We consider *E. coli*'s three antiporters (Fig. 1B) and write the cost as

$$\text{Cost} = j_{H^+} + \sum_a \sigma_{H^+,a} j_a \tag{20}$$

where the flux from leakage is j_{H^+} and from an antiporter a is j_a.

The cost of maintaining a given PMF is minimised by using the antiporter with the smallest value of $\sigma_{H^+,a} j_a$, where the value of j_a is determined by Eq. (6) and Eq. (17) (*Supplementary Information*). The result is that cells should use each antiporter in a specific range of pH_e (Fig. 4A & B): ClcA in a pH_e between approximately 2 and 5; NhaB between 5 and 9; and NhaA between 9 and 12. Consistently, ClcA is known to be important at acidic pH [55] and NhaA in alkaline pH [56, 47, 31] – NHaA's activity increases from a pH_e of 6.5 [57].

As pH_e changes so too does the dominant factor in the cost. For an alkaline pH_e, the minimal cost is dominated by the antiporters; at acidic pH_e, it is dominated by the leakage of protons (Fig. 4C & D).

When minimising the cost, we also optimise the concentration and valency of the captive charges. For a small range of pH_e, the cost is minimised by generating $\Delta\psi$ from the

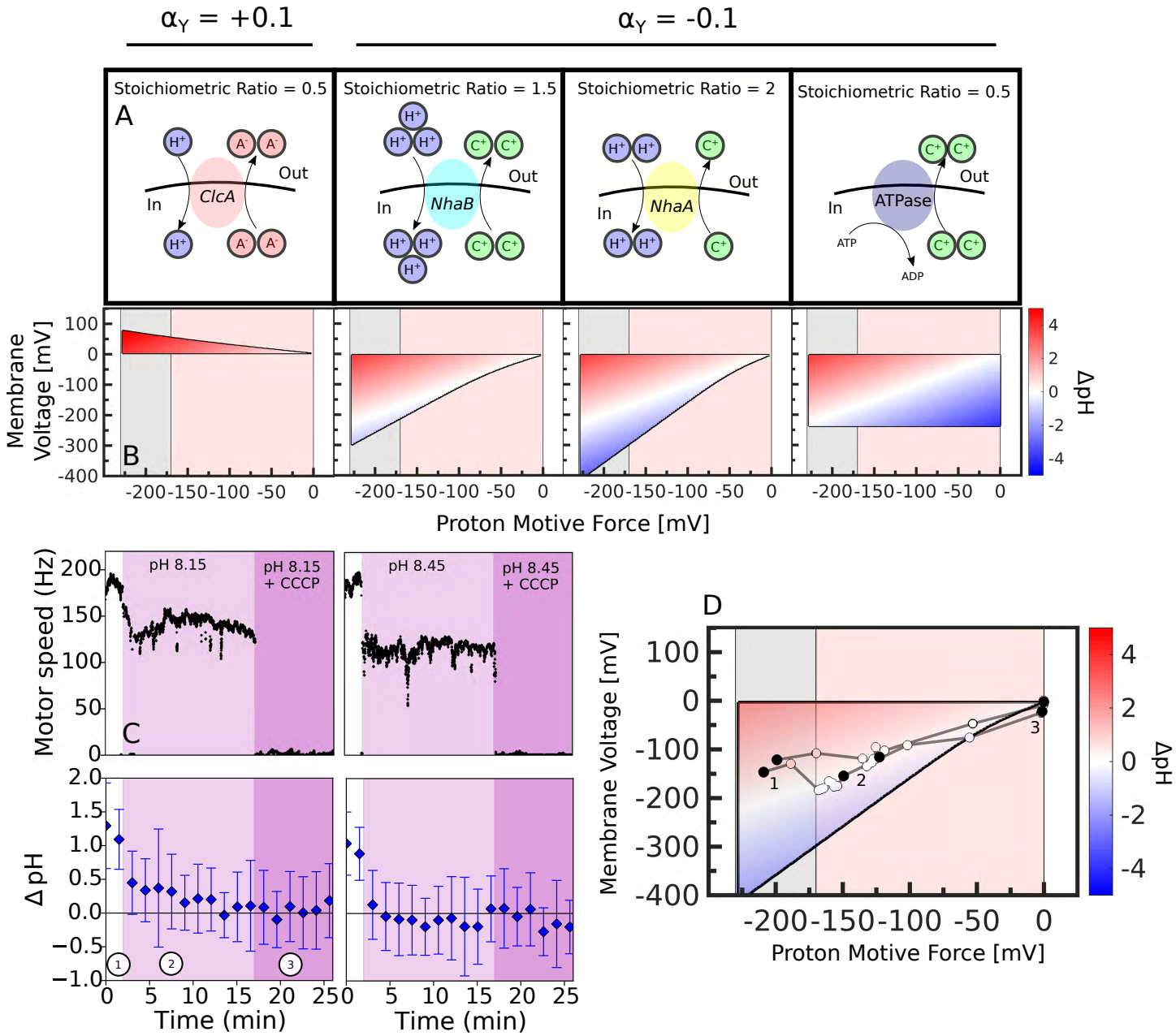

Fig. 3. Proton-ion antiporters are likely to generate the membrane potential in *E. coli.* (A) Schematics of the ionic pumps in the model. We include a hypothetical ATPase with a stoichiometry of one ATP per two cations. (B) Generating $\Delta\psi$ by antiporters or by an ATPase predicts different $\Delta\text{pH} = \text{pH}_i - \text{pH}_e$ when the PMF is close to zero. We plot the possible steady-state membrane potentials as a function of the PMF and show ΔpH using the colour scale with $\text{pH}_i = 7$ (blue is alkaline pH_e; red is acidic). The anionic antiporters maintain a positive potential; the cationic antiporters maintain a negative potential. For computational reasons, we show an approximate $\Delta\psi$ (with an error of $\sim$10 mV – Fig. S9). (C) The single-cell motor speed (top panels), reporting on the dynamics of the PMF, and the average ΔpH (bottom panels) upon alkaline shifts to 8.15 (first column) or 8.45 (second column) followed by addition of a protonophore, CCCP, supports a $\Delta\psi$ generated by antiporters. pH_e is changed from 7 (white – annotated 1) to above 8 (pink – annotated 2) and then CCCP is added (purple – annotated 3). ΔpH is the mean of $\geq$30 cells with standard deviations as errors. (D) The data qualitatively agrees with the model's predictions. We plot data from C in the space of membrane potential versus the PMF obtained for NhaA in B. The PMF is estimated from the motor speed using a conversion factor of 1.13 mV/Hz (Fig. S7) and the membrane potential from Eq. (2). The black annotated dots show specific time points in C. The grey and red shading indicate the respirative and fermentative regimes.

captive charges alone (Fig. 4), but this option is near to equilibrium and likely irrelevant physiologically.

The optimal valency changes sign as pH_e changes (Fig. S10) and should be positive for sufficiently acidic pH_e. This prediction is consistent with observations that cells responds to acidic stress by directly or indirectly generating positive charge: some amino acids to are converted into more positively charged molecules and negatively charged glutamate is converted into neutral γ-aminobutyric acid [58, 59, 60].

Discussion

How bacteria maintain homeostasis has long been of interest. Nevertheless, the key physiological variables – intracellular pH, osmotic pressure, and membrane potential – are typically studied in isolation, despite being interlinked. Here we gain new insights using a model that considers all three simultaneously. We propose that it is the proton-ion antiporters that generate an out-of-equilibrium membrane potential to maintain the PMF. As a consequence, the magnitude of the PMF determines the cell's ability to maintain pH_i as pH_e changes. We demonstrated, in line with predictions, both that a lower magnitude PMF impairs *E. coli*'s maintenance of pH_i (Fig. 2) and that collapsing the PMF depolarises the cell (Fig. 3). These results suggest that the contradictory observations on the dynamics of pH_i, [4, 5, 6] and [7, 8], can be reconciled if one experiment was performed on cells with a lower magnitude PMF, perhaps because of anoxic conditions.

Our assumption that proton-ion antiporters regulate $\Delta\psi$ suggests a shift of perspective away from electrogenicity, the net amount of charge transferred by an ion transporter, to the stoichiometric ratio of a given antiporter. For example, previous work interprets decarboxylation of amino acids as a means to alkalise the cytoplasm by directly consuming intracellular protons [58] and considers NhaA as providing a mechanism to acidify the cytoplasm in alkaline environments by importing protons [1, 47]. Decarboxylation of amino acids from our perspective increases the charge of captive molecules, allowing the membrane potential to shift to more positive values. NhaA, through its higher proton-to-cation stoichiometric ratio than NhaB, generates a more negative $\Delta\psi$ and so preserves both the PMF and pH_i at alkaline pH_e. Even an electroneutral antiporter can generate $\Delta\psi$ [61] contradicting the electrogenic viewpoint [62].

ClcA provides another example of the benefits of changing perspective. Rather than exporting protons to raise pH_i, we predict that ClcA exports chloride ions and imports protons (Fig. 1C & D). ClcA then generates the positive $\Delta\psi$ necessary for the simultaneous maintenance of the PMF and pH_i at sufficiently low pH_e [63, 1]. If ClcA instead exported protons to raise pH_i [29, 64], $\Delta\psi$ would become more negative at acidic pH_e, which is not observed [63].

In contrast, alkalinophiles maintain more negative $\Delta\psi$ compared to neutralophiles [1], and many have proton-sodium antiporters [65]. If those antiporters are responsible for generating the plasma membrane potential, as we suspect, then their distinctive characteristic should be a high proton-to-sodium stoichiometric ratio.

Each type of antiporter has a different energetic cost because even antiporters that catalyse the same type of ionic exchange have different stoichiometric ratios. To reduce costs, we predict that particular antiporters should be expressed for particular ranges of extracellular pH (Fig. 4A). We estimate the cost by the numbers of metabolically pumped protons that are not used to generate ATP and predict that it is a substantial fraction of *E. coli*'s total 'budget' (Fig. 4C). Maintaining chemio-osmotic homeostasis is thought to be a major contributor to cellular maintenance [66] – the energy necessary to run house-keeping processes.

Our work has multiple caveats. We do not address how cells recover the preferred pH_i after a change in extracellular pH, but rather we determine if a steady state with a recovered pH_i is possible. We assume that the cell always has sufficient resources to export protons at a rate to maintain the PMF and pH_i, which may not be true under stress. Finally, our model is deliberately simple, focusing on one type of cation and one type of anion, both with a single charge. Multiple types of ions are of course present in bacteria. Our model remains qualitatively valid if the membrane potential is regulated principally through one type of cation or anion whose driven transport is dominated by one type of antiporter.

Moving away from bacteria, proton-ion antiporters are widespread in nearly all organisms, and defects in these antiporters in mammalian cells are associated with disease [67, 68, 69]). In mammals, the members of the NHE gene family, to which *NhaA* belongs, and the CLC gene family, to which *ClcA* belongs, are also thought to contribute to maintaining cytoplasmic pH [70, 71]. Nevertheless, the multiple compartments of eukaryotic cells may mean that maintaining the PMF between the cytoplasm and extracellular space is not under such strong selection as for bacteria and archaea, and so the activity of proton-ion antiporters may be less constrained.

Methods

Strains and media. For simultaneous measurements of pH_i and the single-cell motor speed we use two strains of *E. coli*. The first is a derivative of MG1655 derivative (EK07 [11]) with sticky filaments and chromosomal expression of pHluorin. The second is the AB1157 strain [46] modified to carry the sticky flagellin encoding gene $fliC^{sticky}$ [40, 11] and transformed with pkk223-3-pHluorin (M153R) plasmid [34]. $FliC^{sticky}$ makes filaments hydrophobic so that they readily stick to polystyrene beads [40]. With the two strains, we confirmed that there are no significant strain-to-strain differences in the behaviour we observe. We used strain EK07 for pH_e=5.5 experiments; strains EK07 and AB1157 for a pH_e of 5.7 and 6.0; strain AB1157 for a pH_e of 4, 4.3, 4.5, 4.7, 5, and 5.3; and strain EK07 for a pH_e of 8.15 and 8.45. Bacteria were diluted ($\times 10^{-3}$) from the frozen overnight culture (OD≈3) and grown in lysogeny broth (LB: 10 g tryptone, 5 g yeast extract, 10 g NaCl per 1 l) in conical flask at 37°C with shaking (220 rpm).

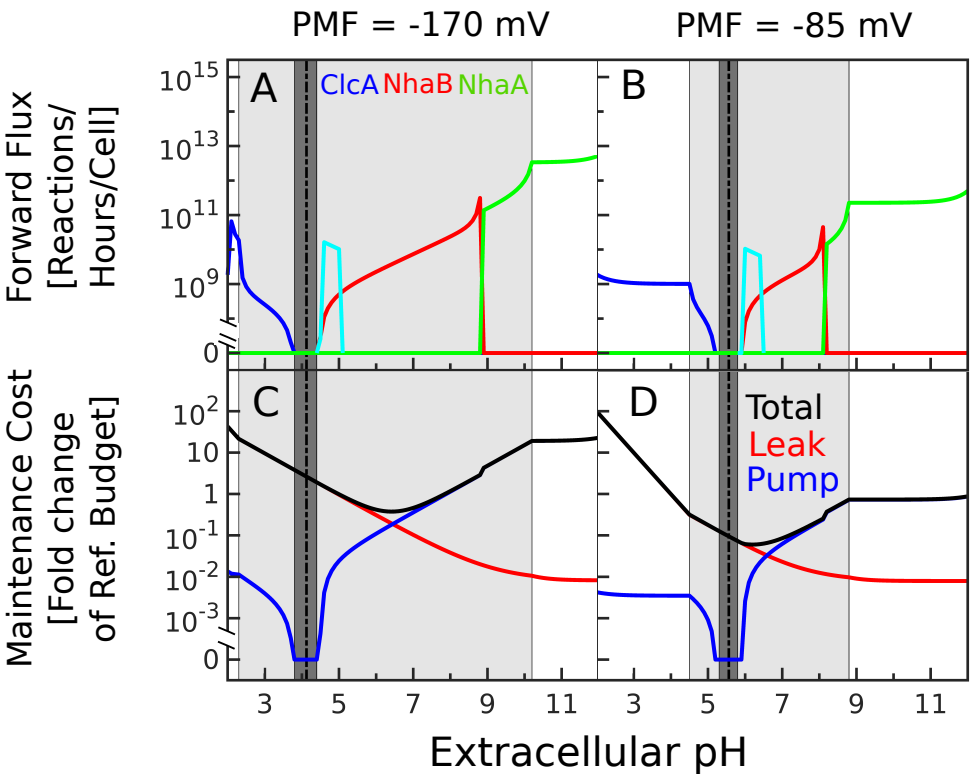

Fig. 4. Maintaining pH_i, the PMF, and osmotic pressure at minimal cost predicts a homeostatic strategy for *E. coli* across different pH_e. We maintain pH_i as close as possible to 7, $-10 \leq z_Y \leq 10$, and set the osmotic pressure to 1 atm and $[CA]_0$ to 50 mM. The black dotted line marks the pH_e for which $\Delta\psi = 0$; to the left, $\Delta\psi > 0$; to the right, $\Delta\psi < 0$. The dark grey indicates where the optimal solution has $\Delta G_{C+} = \Delta G_{A-} = 0$. The light grey area indicates where pH_i can be maintained exactly at 7; to the left, $pH_i < 7$; to the right, $ph_i > 7$. (A,B) For two PMFs, we show the antiporter and its flux that minimises Eq. (20) for different pH_e: ClcA is in blue, NhaB in red, and NhaA in green. The light blue line shows the optimal strategy; the dark blue an approximation (SI). (C,D) For the same PMFs, we show the minimal cost relative to a reference budget (black) of protons per cell per hour, which we estimate for *E. coli* doubling every 60 min aerobically in minimal media supplemented with glucose (SI). We also show the contributions to the cost of the activity of the antiporters (blue) and of leakage (red).

Flagellar motor speed recording and analysis. Cells were harvested at OD= 2.0 to maximise the fraction that expressed the flagellar motor (Spectronic 200E Spectrophotometer, Thermo Scientific, UK). Cells were prepared for microscopy as before [72] using tunnel slides [73]. Experiments were performed in the motility buffer (BMB: aqueous solution of 6.2 mM K_2HPO_4, 3.8 mM KH_2PO_4, 67 mM NaCl, and 0.1 mM EDTA, pH 7.02) supplemented with 20 mM glucose.

For aerobic-anaerobic shifts (Fig. 2B & S5), cells were kept in glucose-supplemented BMB in the tunnel slide, where fresh BMB was flushed in just prior to the recording and the slide was sealed with CoverGrip™ Coverslip Sealant (Biotium, USA) to prevent oxygen diffusion. For experiments presented in Fig. 2 C-F and S6, bead rotation was recorded for 2 min in BMB with glucose in aerobic conditions, at which point the buffer was replaced with the pH-adjusted BMB. The slide was immediately sealed and recording continued for another 30 min. pH 5.5 buffer was adjusted with a mixture of organic acids (0.9 mM acetate, 3.8 mM lactate, 1.4 mM formate and 0.45 mM succinate), whereas the rest of the buffers were pH adjusted using lactic acid only. The choice of the organic acid influences only the dynamics of the drop in motor speed (such as in Fig. 2E), and not the steady speed. The recording of motor speed was uninterrupted for the duration of the experiment (32 min). For alkaline shifts (Fig. 3), we recorded bead rotation for 2 min before flushing BMB adjusted with NaOH to pH 8.15 or 8.45. The slide was not sealed to allow another flush of BMB supplemented with 100 µM CCCP at 17 min and recording was continued for another 10 min.

Relative (x, y) bead coordinates recorded with a position-sensitive detector were converted to the flagellar motor rotational frequencies by applying a flat-top discrete Fourier transform with 1.6384 s window and 0.1 s step size [11, 42]. The resulting time series were median-filtered with the additional removal of 50 Hz AC frequency values and values below 10 Hz [11, 42].

Intracellular pH measurements. The intracellular pH of the bacteria was measured with ratiometric pHluorin [74, 39] using an established imaging protocol and sensor calibration [75]. Images were taken every 90 s with 50 ms exposure time.

Fluorescence images of pHluorin were analysed as before [11, 39]. An Otsu threshold followed by binary erosion and binary dilation was applied to both 475 nm and 395 nm excitation images, and the mean intensity was calculated for each cell in both channels. The ratio of these values with the background subtracted was later converted to pH units using a calibration curve generated following [39].

Computational results. The computational algorithms are described in the *Supplementary Information*. To numerically solve the steady-state equations we used the MATLAB function `vpasolve`.

Availability of data. Our experimental data is available at https://datashare.is.ed.ac.uk/handle/10283/2058.

ACKNOWLEDGEMENTS

We would like to thank all members of the Pilizota and Swain labs as well as Sebastian Jaramillo-Riveri, Xavier Zaoui, Vincent Danos, Joshua Shaevitz, Ariel Amir, and Calin Guet for support and useful discussions. We would like to thank Joanne Slonezewski and Linda Kenny for providing and helping us with reproducing their previously published data in Fig. 1A. TP, GT and EK were supported by the Human Frontier Science Program grant (RGP0041/2015), GT is supported by the Darwin Trust of the University of Edinburgh, and PSS by the BBSRC.

Bibliography

References

1. Terry A. Krulwich, George Sachs, and Etana Padan. Molecular aspects of bacterial pH sensing and homeostasis. *Nature Reviews*, 2011.

2. Wataru Aoi and Yoshinori Marunaka. Importance of pH homeostasis in metabolic health and diseases: crucial role of membrane proton transport. *BioMed research international*, 2014:598986–598986, 2014. PMC4180894[pmcid].

3. An-Suei Yang and Barry Honig. On the pH dependence of protein stability. *Journal of Molecular Biology*, 231(2):459 – 474, 1993.

4. Joan L. Slonczewski, Robert M. Macnab, Jeffry R. Alger, and Anna M. Castle. Effects of pH and repellent tactic stimuli on protein methylation levels in Escherichia coli. *Journal of Bacteriology*, 152(1):384–399, 1982.

5. Jessica C. Wilks and Joan L. Slonczewski. pH of the cytoplasm and periplasm of Escherichia coli: Rapid measurement by green fluorescent protein fluorimetry. *Journal of Bacteriology*, 189(15):5601–5607, 2007.

6. Keith A. Martinez, Ryan D. Kitko, J. Patrick Mershon, Haley E. Adcox, Kotiba A. Malek, Melanie B. Berkmen, and Joan L. Slonczewski. Cytoplasmic pH response to acid stress in individual cells of Escherichia coli and Bacillus subtilis observed by fluorescence ratio imaging microscopy. *Applied and Environmental Microbiology*, 78(10):3706–3714, 2012.

7. Smarajit Chakraborty, Ricksen S. Winardhi, Leslie K. Morgan, Jie Yan, and Linda J. Kenney. Non-canonical activation of OmpR drives acid and osmotic stress responses in single bacterial cells. *Nature Communications*, 8(1):1587, 2017.

8. Smarajit Chakraborty and Linda J. Kenney. A new role of OmpR in acid and osmotic stress in Salmonella and E. coli. *Frontiers in Microbiology*, 9:2656, 2018.

9. Andrew Tze Fui Liew, Yong Hwee Foo, Yunfeng Gao, Parisa Zangoui, Moirangthem Kiran Singh, Ranjit Gulvady, and Linda J Kenney. Single cell, super-resolution imaging reveals an acid pH-dependent conformational switch in SsrB regulates SPI-2. *eLife*, 8:e45311, April 2019.

10. Janet M. Wood. Bacterial responses to osmotic challenges. *The Journal of general physiology*, 145(5):381–388, May 2015. PMC4411257[pmcid].

11. Ekaterina Krasnopeeva, Chien-Jung Lo, and Teuta Pilizota. Single-cell bacterial electrophysiology reveals mechanisms of stress-induced damage. *Biophysical Journal*, 116(12):2390 – 2399, 2019.

12. Leonardo Mancini, Guillaume Terradot, Tian Tian, Ying Ying Pu, Yingxing Li, Chien Jung Lo, Fan Bai, and Teuta Pilizota. A general workflow for characterization of nernstian dyes and their effects on bacterial physiology. *Biophysical Journal*, 2019.

13. J. Keener and J. Sneyd. *Mathematical Physiology*. 2009.

14. Bryson D. Bennett, Elizabeth H. Kimball, Melissa Gao, Robin Osterhout, Stephen J. Van Dien, and Joshua D. Rabinowitz. Absolute metabolite concentrations and implied enzyme active site occupancy in Escherichia coli. *Nat Chem Biol*, 5(8):593–599, Aug 2009.

15. Tomoya Honda, Jonas Cremer, Leonardo Mancini, Zhongge Zhang, Teuta Pilizota, and Terence Hwa. Tight coordination of gene expression with cell size enables Escherichia coli to efficiently maintain motility across conditions. *Submitted*, 2021.

16. Jonas Cremer, Tomoya Honda, Ying Tang, Jerome Wong-Ng, Massimo Vergassola, and Terence Hwa. Chemotaxis as a navigation strategy to boost range expansion. *Nature*, 575(7784):658–663, nov 2019.

17. Daniel A Beard and Hong Qian. *Chemical biophysics: quantitative analysis of chemical systems*. Cambridge University Press, Cambridge, U. K., 2006.

18. Enrique Rojas, Julie A. Theriot, and Kerwyn Casey Huang. Response of escherichia coli growth rate to osmotic shock. *Proceedings of the National Academy of Sciences*, 111(21):7807–7812, 2014.

19. Daniel A Beard and Hong Qian. Relationship between thermodynamic driving force and one-way fluxes in reversible processes. *PloS one*, 2(1):e144, 2007.

20. Keith D. Garlid, Andrew D. Beavis, and Signe K. Ratkje. On the nature of ion leaks in energy-transducing membranes. *Biochimica et Biophysica Acta (BBA) - Bioenergetics*, 976(2):109 – 120, 1989.

21. P. Mitchell. Coupling of phosphorylation to electron and hydrogen transfer by a chemi-osmotic type of mechanism. *Nature*, 191(4784):144–148, Jul 1961.

22. Stefan Steigmiller, Paola Turina, and Peter Gräber. The thermodynamic H+/ATP ratios of the H+-ATPsynthases from chloroplasts and Escherichia coli. *Proceedings of the National Academy of Sciences*, 105(10):3745–3750, 2008.

23. Avi Flamholz, Elad Noor, Arren Bar-Even, and Ron Milo. eQuilibrator—the biochemical thermodynamics calculator. *Nucleic Acids Research*, 40(D1):D770–D775, 11 2011.

24. P.R. Rich. The molecular machinery of Keilin's respiratory chain. *Biochemical Society Transactions*, 31(6):1095–1105, 12 2003.

25. David B. Hicks, Jun Liu, Makoto Fujisawa, and Terry A. Krulwich. F1F0-ATP synthases of alkaliphilic bacteria: Lessons from their adaptations. *Biochimica et Biophysica Acta (BBA) - Bioenergetics*, 1797(8):1362 – 1377, 2010.

26. Christoph von Ballmoos, Alexander Wiedenmann, and Peter Dimroth. Essentials for ATP synthesis by F1F0 ATP synthases. *Annual Review of Biochemistry*, 78(1):649–672, 2009. PMID: 19489730.

27. Terry J. Beveridge. Structures of gram-negative cell walls and their derived membrane vesicles. *Journal of Bacteriology*, 181(16):4725–4733, 1999.

28. Chien-Jung Lo, Mark C. Leake, Teuta Pilizota, and Richard M. Berry. Nonequivalence of membrane voltage and ion-gradient as driving forces for the bacterial flagellar motor at low load. *Biophysical Journal*, 93(1):294–302, Jul 2007.

29. Alessio Accardi and Christopher Miller. Secondary active transport mediated by a prokaryotic homologue of ClC Cl- channels. *Nature*, 427(6977):803–807, Feb 2004.

30. E Pinner, E Padan, and S Schuldiner. Kinetic properties of NhaB, a Na+/H+ antiporter from Escherichia coli. *Journal of Biological Chemistry*, 269(42):26274–26279, 1994.

31. D Taglicht, E Padan, and S Schuldiner. Proton-sodium stoichiometry of NhaA, an electrogenic antiporter from Escherichia coli. *Journal of Biological Chemistry*, 268(8):5382–7, 1993.

32. D. Scott Cayley, Harry J. Guttman, and M. Thomas Record. Biophysical characterization of changes in amounts and activity of Escherichia coli cell and compartment water and turgor pressure in response to osmotic stress. *Biophysical Journal*, 78(4):1748–1764, April 2000.

33. Yi Deng, Mingzhai Sun, and Joshua W. Shaevitz. Direct measurement of cell wall stress stiffening and turgor pressure in live bacterial cells. *Phys. Rev. Lett.*, 107:158101, Oct 2011.

34. Yusuke V. Morimoto, Seiji Kojima, Keiichi Namba, and Tohru Minamino. M153R mutation in a pH-sensitive green fluorescent protein stabilizes its fusion proteins. *PLoS ONE*, 6(5):e19598, 2011.

35. Ekaterina Krasnopeeva, Uriel E. Barboza-Perez, Jerko Rosko, Teuta Pilizota, and Chien-Jung Lo. Bacterial flagellar motor as a multimodal biosensor. *Methods*, page S1046202320301328, July 2020.

36. Yoshiyuki Sowa and Richard M Berry. Bacterial flagellar motor. *Q. Rev. Biophys.*, 41(2):103–132, 2008.

37. David C. Fung and Howard C. Berg. Powering the flagellar motor of Escherichia coli with an external voltage source. *Nature*, 375(6534):809–812, 1995.

38. Christopher V Gabel and Howard C Berg. The speed of the flagellar rotary motor of Escherichia coli varies linearly with protonmotive force. *Proc. Natl. Acad. Sci. U. S. A.*, 100(15):8748–8751, jul 2003.

39. Yao Kuan Wang, Ekaterina Krasnopeeva, Ssu-Yuan Lin, Fan Bai, Teuta Pilizota, and Chien-Jung Lo. Comparison of Escherichia coli surface attachment methods for single-cell microscopy. *Scientific Reports*, 9(December):2019, dec 2019.

40. G Kuwajima. Construction of a minimum-size functional flagellin of Escherichia coli. *J. Bacteriol.*, 170(7):3305–3309, jul 1988.

41. William S. Ryu, Richard M. Berry, and Howard C. Berg. Torque-generating units of the flagellar motor of Escherichia coli have a high duty ratio. *Nature*, 403(6768):444–447, jan 2000.

42. Jerko Rosko, Vincent Martinez, Wilson Poon, and Teuta Pilizota. Osmotaxis in Escherichia coli through changes in motor speed. *Proc. Natl. Acad. Sci. U. S. A.*, 114(38):E7969–E7976, 2017.

43. Karel Svoboda, Christoph F. Schmidt, Bruce J. Schnapp, and Steven M. Block. Direct observation of kinesin stepping by optical trapping interferometry. *Nature*, 365(6448):721–727, oct 1993.

44. Winfried Denk and Watt W. Webb. Optical measurement of picometer displacements of transparent microscopic objects. *Appl. Opt.*, 29(16):2382–2391, jun 1990.

45. Renata Buda, Yunxiao Liu, Jin Yang, Smitha Hegde, Keiran Stevenson, Fan Bai, and Teuta Pilizota. Dynamics of Escherichia coli 's passive response to a sudden decrease in external osmolarity. *Proc. Natl. Acad. Sci. U. S. A.*, 113(40):E5838–E5846, oct 2016.

46. Jana Schwarz-Linek, Jochen Arlt, Alys Jepson, Angela Dawson, Teun Vissers, Dario Miroli, Teuta Pilizota, Vincent A. Martinez, and Wilson C.K. Poon. Escherichia coli as a model active colloid: A practical introduction. *Colloids and Surfaces B: Biointerfaces*, 137:2–16, jan 2016.

47. Etana Padan, Eitan Bibi, Masahiro Ito, and Terry A. Krulwich. Alkaline pH homeostasis in bacteria: New insights. *Biochimica et Biophysica Acta (BBA) - Biomembranes*, 1717(2):67 – 88, 2005.

48. Terry A. Krulwich, David B. Hicks, and Masahiro Ito. Cation/proton antiporter complements of bacteria: why so large and diverse? *Molecular Microbiology*, 74(2):257–260, 2009.

49. Jack H. Kaplan. Biochemistry of Na,K-ATPase. *Annual Review of Biochemistry*, 71(1):511–535, 2002. PMID: 12045105.

50. Ben Z. Cavari and Y. Avi-Dor. Effect of carbonyl cyanide m-chlorophenylhydrazone on respiration and respiration-dependent phosphorylation in Escherichia coli. *The Biochemical Journal*, 103(2):601–608, 1967.

51. Dai Le, Ekaterina Krasnopeeva, Faris Sinjab, Teuta Pilizota, and Minsu Kim. Active efflux leads to heterogeneous dissipation of proton motive force by protonophores in bacteria. *mBio, Accepted/In Press*, June 2021.

52. D Zilberstein, V Agmon, S Schuldiner, and E Padan. Escherichia coli intracellular pH, membrane potential, and cell growth. *Journal of Bacteriology*, 158(1):246–252, 1984.

53. Robert I. Macey, Joseph S. Adorante, and Frank W. Orme. Erythrocyte membrane potentials determined by hydrogen ion distribution. *Biochimica et Biophysica Acta (BBA) - Biomembranes*, 512(2):284 – 295, 1978.

54. Poul Bennekou and Palle Christophersen. Flux ratio of valinomycin-mediated K+ fluxes across the human red cell membrane in the presence of the protonophore CCCP. *The Journal of Membrane Biology*, 93(3):221–227, Oct 1986.

55. Ramkumar Iyer, Tina M. Iverson, Alessio Accardi, and Christopher Miller. A biological role for prokaryotic ClC chloride channels. *Nature*, 419(6908):715–718, 2002.

56. Etana Padan. The enlightening encounter between structure and function in the NhaA Na+ – H+ antiporter. *Trends in Biochemical Sciences*, 33(9):435 – 443, 2008.

57. D Taglicht, E Padan, and S Schuldiner. Overproduction and purification of a functional Na+/H+ antiporter coded by nhaA (ant) from Escherichia coli. *Journal of Biological Chemistry*, 266(17):11289–11294, 1991.

58. Usheer Kanjee and Walid A. Houry. Mechanisms of Acid Resistance in *Escherichia coli*. *Annual Review of Microbiology*, 67(1):65–81, September 2013.

59. Eugenia Pennacchietti, Fabio Giovannercole, and Daniela De Biase. Acid survival mechanisms in neutralophilic bacteria. In *Stress and Environmental Regulation of Gene Expression and Adaptation in Bacteria*, pages 911–926. John Wiley & Sons, Ltd, 2016.

60. J. Lin, M. P. Smith, K. C. Chapin, H. S. Baik, G. N. Bennett, and J. W. Foster. Mechanisms of acid resistance in enterohemorrhagic Escherichia coli. *Applied and Environmental Microbiology*, 62(9):3094–3100, September 1996.

61. R. Jacob, D. Piwnica-Worms, C. R. Horres, and M. Lieberman. Theoretical effects of transmembrane electroneutral exchange on membrane potential. *The Journal of general physiology*, 83(1):47–56, Jan 1984. PMC2215621[pmcid].

62. Gerardo Gamba. Molecular physiology and pathophysiology of electroneutral cation-chloride cotransporters. *Physiological Reviews*, 85(2):423–493, 2005. PMID: 15788703.

63. Richard Hope and John W. Foster. Escherichia coli glutamate- and arginine-dependent acid resistance systems increase internal pH and reverse transmembrane potential. *Journal of Bacteriology*, 186(18):6032–6041, 2004.

64. Christopher Miller and Wang Nguitragool. A provisional transport mechanism for a chloride channel-type Cl-/H+ exchanger. *Philosophical Transactions of the Royal Society B: Biological Sciences*, 364(1514):175–180, 2009.

65. Terry Ann Krulwich, Jun Liu, Masato Morino, Makoto Fujisawa, Masahiro Ito, and David B. Hicks. *Adaptive Mechanisms of Extreme Alkaliphiles*, pages 119–139. Springer Japan, Tokyo, 2011.

66. Peter van Bodegom. Microbial maintenance: A critical review on its quantification. *Microbial Ecology*, 53(4):513–523, 2007.

67. Daniel G. Fuster and R. Todd Alexander. Traditional and emerging roles for the SLC9 Na+/H+ exchangers. *Pflügers Archiv - European Journal of Physiology*, 466(1):61–76, 2014.

68. M. Schwede, K. Garbett, K. Mirnics, D. H. Geschwind, and E. M. Morrow. Genes for endosomal NHE6 and NHE9 are misregulated in autism brains. *Molecular Psychiatry*, 19(3):277–279, 2014.

69. Maya Schushan, Minghui Xiang, Pavel Bogomiakov, Etana Padan, Rajini Rao, and Nir Ben-Tal. Model-guided mutagenesis drives functional studies of human NHA2, implicated in hypertension. *Journal of Molecular Biology*, 396(5):1181 – 1196, 2010.

70. P. G. Vallés, V. Bocanegra, A. Gil Lorenzo, and V. V. Costantino. Physiological functions and regulation of the Na+/H+ exchanger [NHE1] in renal tubule epithelial cells. *Kidney and Blood Pressure Research*, 40(5):452–466, 2015.

71. Yoichi Ishida, Smita Nayak, Joseph A Mindell, and Michael Grabe. A model of lysosomal pH regulation. *The Journal of general physiology*, 141(6):705—720, June 2013.

72. Teuta Pilizota, Jerko Rosko, and Ekaterina Krasnopeeva. BFM speed recording with back-focal-plane interferometry. *dx.doi.org/10.17504/protocols.io.bch2it8e*, March 2021.

73. Uriel Barboza Perez, Ekaterina Krasnopeeva, Jerko Rosko, and Teuta Pilizota. Tunnel slide preparation for motor speed recordings. *dx.doi.org/10.17504/protocols.io.bcjdiui6*, March 2021.

74. Gero Miesenböck, Dino A. De Angelis, and James E. Rothman. Visualizing secretion and synaptic transmission with pH-sensitive green fluorescent proteins. *Nature*, 394(6689):192–195, 1998.

75. Ekaterina Krasnopeeva and Teuta Pilizota. Cytoplasmic pH measurements with pHluorin. *dx.doi.org/10.17504/protocols.io.bhi7j4hn*, March 2021.